Polymer 50 (2009) 605–612

Contents lists available at ScienceDirect

Polymer

journal homepage: www.elsevier.com/locate/polymer

Electrospun polyacrylonitrile/zinc chloride composite nanofibers and their response to hydrogen sulfide

Liwen Ji, Andrew J. Medford, Xiangwu Zhang*

Fiber and Polymer Science Program, Department of Textile Engineering, Chemistry and Science, North Carolina State University, 2401 Research Drive, Box 8301, Raleigh, NC 27695-8301, USA

ARTICLE INFO

Article history:
Received 12 September 2008
Received in revised form
3 November 2008
Accepted 8 November 2008
Available online 24 November 2008

Keywords:
Electrospinning
Polyacrylonitrile
Zinc(II) chloride

ABSTRACT

In this work, we explore the electrospinning of polyacrylonitrile (PAN)/zinc(II) chloride ($ZnCl_2$) composite nanofibers and the response of these nanofibers to hydrogen sulfide (H_2S). Solution properties, including surface tension, viscosity, and conductivity, have been measured and integrated with the results of a variety of other analytical techniques to investigate the effects of $ZnCl_2$ salt on the structure and thermal properties of electrospun nanofibers. It is found that the addition of $ZnCl_2$ reduces the diameter and inhibits the instantaneous cyclization reaction of these nanofibers. Additionally, exposing PAN/$ZnCl_2$ fibers to H_2S leads to the formation of PAN/zinc sulfide (ZnS) composite nanofibers that contain ZnS crystals on the surface. These results indicate that PAN/$ZnCl_2$ composite nanofibers could find applications in H_2S sensing and removal, or as precursors for semiconductor ZnS-coated polymer nanofibers.

1. Introduction

One-dimensional nanostructured materials with a variety of forms, such as nanotubes, nanowires, nanobelts, and nanofibers, are of great interest due to their unique properties and intriguing applications in many fields [1]. Among various methods to prepare these materials, electrospinning is currently one of the most versatile and promising processes for producing continuous nanofibers for both fundamental and application-oriented research mainly due to its capability and feasibility in generating large quantities of nanofibers with well-defined surface topologies at relatively low cost [1–4].

Recently, tremendous work has focused on the dispersion of inorganic salts or nanoparticles into electrospun polymer nanofibers due to the fact that such nanofibers allow a unique blend of properties, such as good mechanical strength and heat stability of inorganic materials, and excellent flexibility and moldability of polymers, while they still can maintain other functional properties of either constituent. Among various polymer/inorganic composite nanofibers, polymer/transition-metal salt composite nanofibers have attracted attention primarily due to the fact that these fibers can be easily transformed into polymer/metal or polymer/semiconductor composite nanofibers through subsequent chemical treatment [5–8]. Nanofibers of this nature have many potential applications, such as photographic and optical materials, catalysis and catalyst supports, ionic conductors, sensors, and environmental protection materials [1,6–10].

In this paper, we report the incorporation of zinc chloride ($ZnCl_2$) salts into electrospun polymer nanofibers to form a new type of functional material. $ZnCl_2$ is an important zinc halide agent which is often used to prepare activated carbon materials with ultrahigh surface areas [11]. Additionally, $ZnCl_2$ can react with H_2S to form a metal sulfide precipitate, i.e., ZnS, a direct wide band gap semiconductor with a large excitation binding energy and a small Bohr radius [12–14]. As a result, after incorporating $ZnCl_2$ into polymer nanofibers, the high surface-area-to-volume-ratio of these nanofiber-based materials can facilitate the diffusion of H_2S into the nanofiber matrix, where H_2S can react with $ZnCl_2$ to produce ZnS, altering the electrical response of the fibers, and HCl as the by-product. Therefore, $ZnCl_2$-added polymer nanofibers are potential material candidates for use in sensing and removing H_2S, which is colorless, flammable, heavier than air, and dangerous to the environment and human health. In addition, $ZnCl_2$-added polymer nanofibers are excellent precursors for preparing ZnS containing nanofibers, which show eminent prospects and opportunities for new applications in a wide variety of areas, such as catalysts, electronic and optoelectronic nanodevices, due to the unique catalytic and semiconducting properties of ZnS [12–14].

Current research efforts have focused on the fabrication and characterization of $ZnCl_2$-added PAN nanofibers and their response to H_2S aqueous solutions. The procedure involves using PAN

* Corresponding author. Tel.: +1 919 515 6547; fax: +1 919 515 6532.
E-mail address: xiangwu_zhang@ncsu.edu (X. Zhang).

0032-3861/$ – see front matter © 2008 Elsevier Ltd. All rights reserved.
doi:10.1016/j.polymer.2008.11.016

solutions in *N*, *N*-dimethylformamide (DMF) containing different amounts of $ZnCl_2$ to prepare composite nanofibers via electrospinning. In order to examine the response of these composite nanofibers to H_2S, PAN/$ZnCl_2$ nanofibers were exposed to H_2S aqueous solution and a variety of characterization methods indicate the formation of PAN/ZnS nanofibers. This technique may also be applicable to other transition-metal ions, such as Cu^{2+}, Cd^{2+}, and Ag^{+}, etc. Salts of these transition metals can also be electrospun through processes analogous to the procedure indicated here. These metal salt-loaded composite nanofibers may have applications in a variety of fields.

2. Experimental

2.1. Materials

PAN ($M_w = 150{,}000$), $ZnCl_2$ (99.995%, powder, anhydrous), H_2S water solution (0.4 g H_2S per 100 ml solution), and solvent DMF were purchased from Aldrich Chemical Company Inc. (USA), and all were used as-received without further purification.

2.2. Preparation of electrospinning solutions

DMF solutions of PAN (7 wt%) containing various amount of $ZnCl_2$ (0, 1, 2, 5, 10, and 15 wt%) were prepared at 60 °C. Mechanical stirring was applied for at least 24 h to form homogeneous solutions.

2.3. Property measurements of electrospinning solutions

The surface tension of solutions was measured by a surface-tension tensiometer (Fisher Scientific, model 21) at room temperature, and the solution conductivity was measured using a potentiostat (Gamry Reference 600). The viscosity measurements were performed at room temperature in a stress-controlled rheometer (TA Instruments AR-2000) using primarily cone and plate geometry. Reproducibility of these solution properties was assessed by conducting all measurements on at least nine samples.

2.4. Preparation of PAN/$ZnCl_2$ nanofibers

A variable high voltage power supply (Gamma ES40P-20W/DAM) was used to provide a spinning voltage of 14 kV. Electrospinning solutions were loaded in a 10 ml syringe, to which a stainless steel capillary metal-hub needle was attached. The inner diameter of the metal needle was 0.30 mm. The positive electrode of the high voltage power supply was connected to the needle tip. The grounded electrode was connected to a metallic collector covered with an aluminum foil. The tip-collector distance and flow rate were fixed at 15 cm and 0.5 ml h^{-1}, respectively. Under high voltage, a polymer jet was ejected and accelerated toward the counter electrode, during which the solvent was rapidly evaporated. Dry fibers were accumulated on the aluminum surface and collected as a fibrous mat.

2.5. Exposure of PAN/$ZnCl_2$ nanofibers to H_2S

PAN/ZnS composite nanofibers were prepared by soaking PAN/$ZnCl_2$ composite nanofibers in a H_2S water solution (0.4 g H_2S per 100 ml) for 1 h, followed by washing with deionized water for several times and vacuum drying at room temperature.

2.6. Morphologies of composite nanofibers

The morphology and diameter of electrospun nanofibers were evaluated using scanning electron microscopy (JEOL 6400F Field Emission SEM at 5 kV). Electrospun samples were coated with Au/Pd layers of approximately 100 Å thick by a K-550X sputter coater to reduce charging. Transmission electron microscopy (Hitachi HF-2000 TEM at 200 kV and FEI Tecnai G^2 Twin at 120 kV) was also used to study the structure of nanofibers collected on 200 mesh carbon-coated Cu grids. The diameters of electrospun nanofibers were determined by measuring 62 randomly selected fibers using the Revolution software package.

2.7. ATR-FTIR spectroscopy

Attenuated total reflection Fourier transform infrared (ATR-FTIR) spectra were collected from a FTIR spectrometer (Nicolet 560) in the wavenumber range of 4000–400 cm^{-1} at room temperature. At least 32 scans were conducted to achieve an adequate signal-to-noise ratio.

2.8. Thermal analysis

Thermal properties of electrospun fibers were evaluated using differential scanning calorimetry (DSC) from 25 to 400 °C at a heating rate of 10 °C min^{-1} in a nitrogen environment (Perkin Elmer Diamond Series DSC with Intracooler). Thermo-gravimetric analysis (TGA) was also used to determine the weight loss of composite nanofibers (after solvent evaporation) at 10 °C min^{-1} from 25 to 800 °C in an air environment (TA Instruments Hi-Res TGA 2950).

2.9. WAXD patterns

Wide-angle X-ray diffraction (WAXD) analysis was performed with a Siemens D5000 using Cu Kα radiation. The operating voltage and current were 40.0 kV and 60.0 mA, respectively. The diffractometer used was a Philips 1050/81. A crystal-monochromated collection system was used to acquire the diffractogram at 0.02° intervals at a rate of 1 s per step. Peak positions were determined by the APD 1700 (Version 4) software.

2.10. UV–vis spectra

Ultraviolet–visible (UV–vis) spectra of PAN/ZnS composite nanofiber-based films were recorded using a Varian UV–vis spectrophotometer with absorption spectra in the range 800–100 nm.

3. Results and discussion

3.1. PAN/$ZnCl_2$ nanofiber diameter and morphology

Fig. 1 shows SEM images and diameter distribution curves of PAN/$ZnCl_2$ composite nanofibers electrospun from 7 wt% PAN solutions with different $ZnCl_2$ concentrations (0, 5, 10, and 15 wt%) at a fixed voltage of 14 kV. It is seen that all fibers are relatively uniform and randomly oriented, forming an interwoven network on the substrate. Defects, such as beads or fibers with 'beads on a string' morphology [15], can seldom be seen when the $ZnCl_2$ concentration is lower than 15 wt%. A small number of bead-like irregularities appear in the nanofibers spun from solutions with 15 wt% $ZnCl_2$ concentration, and the diameters of these nanofibers exhibit a bimodal distribution (i.e., two peaks in the fiber diameter distribution curve, Fig. 1d). Additionally, the average diameters of composite nanofibers gradually decrease from 290 to 250, 180, and 130 nm when $ZnCl_2$ concentration increases from 0 to 5, 10, and

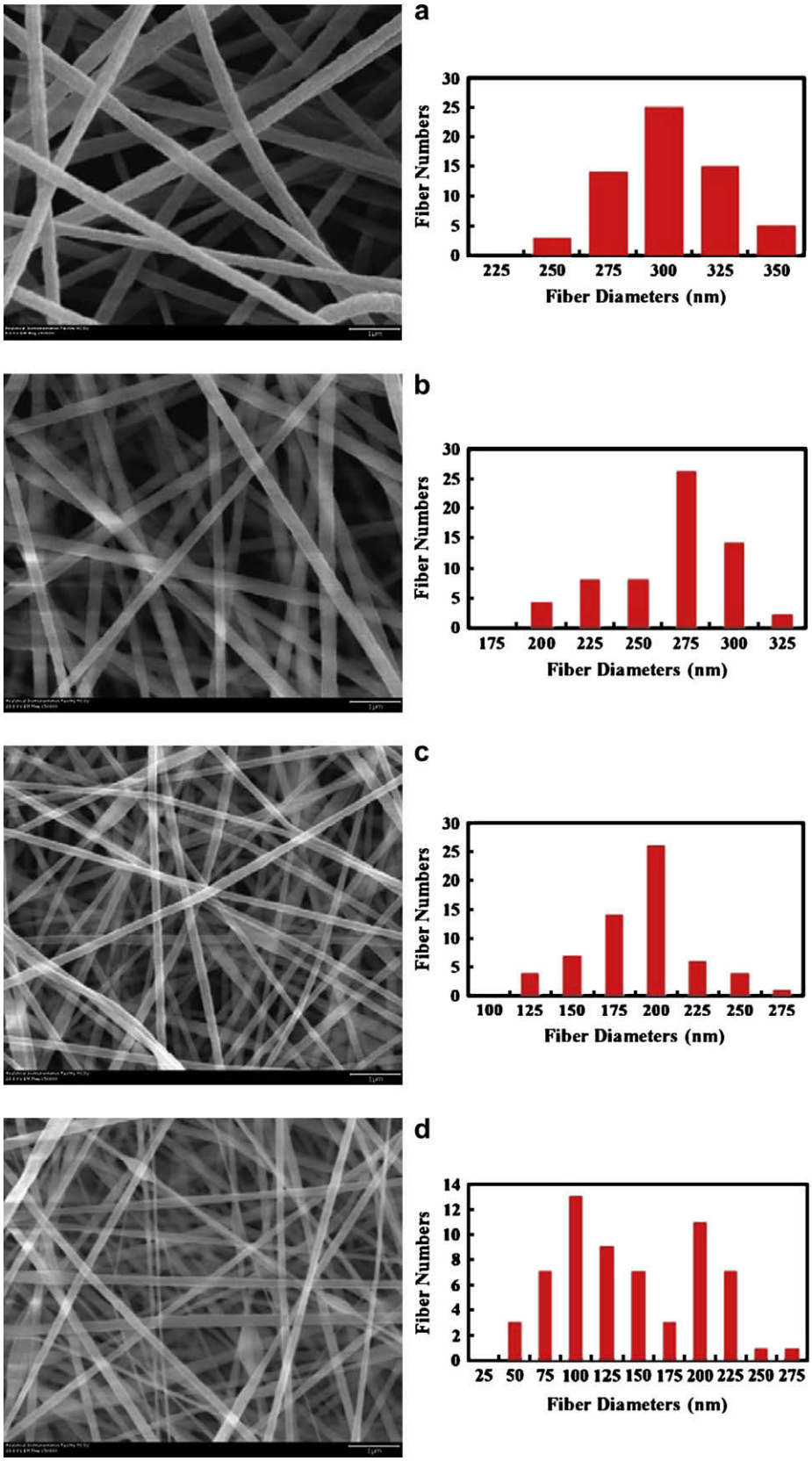

Fig. 1. SEM images and diameter distributions of PAN/$ZnCl_2$ composite nanofibers with different $ZnCl_2$ concentrations: (a) 0 (pure PAN), (b) 5, (c) 10, and (d) 15 wt%.

Table 1
Characteristics of PAN/$ZnCl_2$ electrospinning solutions.

$ZnCl_2$ (wt%)	Viscosity[a] (PaS)	Surface tension[b] (Dyn/cm)	Conductivity (μs/cm)	Diameter[a] (nm)
0	0.26	35.5 ± 0.5	58.7	290 ± 20
5	0.29	36.7 ± 0.3	160.3	250 ± 30
10	0.31	37.3 ± 0.4	251.1	180 ± 30
15	0.34	37.7 ± 0.5	330.2	130 ± 60

[a] Shear rate is about 1.8 S^{-1}.
[b] Values are expressed as means ± SD.

15 wt%, respectively. Nanofiber diameter is typically influenced by the viscosity, surface tension, and conductivity of the electrospinning solution [1–4]. To understand the relationship between nanofiber diameter and $ZnCl_2$ concentration, the viscosity, surface tension, and conductivity were measured for all electrospinning solutions and are shown in Table 1. It is seen that, with increase in $ZnCl_2$ concentration, the solution viscosity increases (e.g., an increase of 31% when $ZnCl_2$ concentration increases from 0 to 15 wt%), which can be explained by interactions among PAN molecules, $ZnCl_2$ salt, and DMF solvent. The polymer–salt–solvent interactions are confirmed by the ATR-FTIR results, which will be discussed later. As shown in Table 1, with increasing $ZnCl_2$ concentration, there is also a slight increase in surface tension (e.g., an increase of 6% when $ZnCl_2$ concentration increases from 0 to 15 wt%). This is likely another result of the interactions among PAN, $ZnCl_2$, and DMF. In addition, Table 1 shows a dramatic influence of $ZnCl_2$ on solution conductivity. Conductivity increases from 58.7 μs/cm (pure PAN) to 330.2 μs/cm (15 wt% $ZnCl_2$ solution) since more free ions are available at higher $ZnCl_2$ concentration. This distinct change (an increase of 460%) in solution conductivity is significantly greater than that of viscosity (31%) and surface tension (6%). Therefore, the decrease of nanofiber diameters with increasing $ZnCl_2$ concentration should be attributed predominantly to the increased conductivity of the polymer solutions. The increased conductivity of the polymer solution can cause an increase in net charge density, and hence a larger force of electrostatic repulsion. The massive increase in electrostatic repulsion, compared to the small changes of surface tension and viscosity, tends to increase the surface area, which opposes the formation of spheres and leads to a decrease in fiber diameters [1–4]. TEM images of the PAN/$ZnCl_2$ (10%) composite nanofibers are displayed in Fig. 2. These images further demonstrate the relatively uniform and randomly oriented morphology of electrospun PAN/$ZnCl_2$ nanofibers.

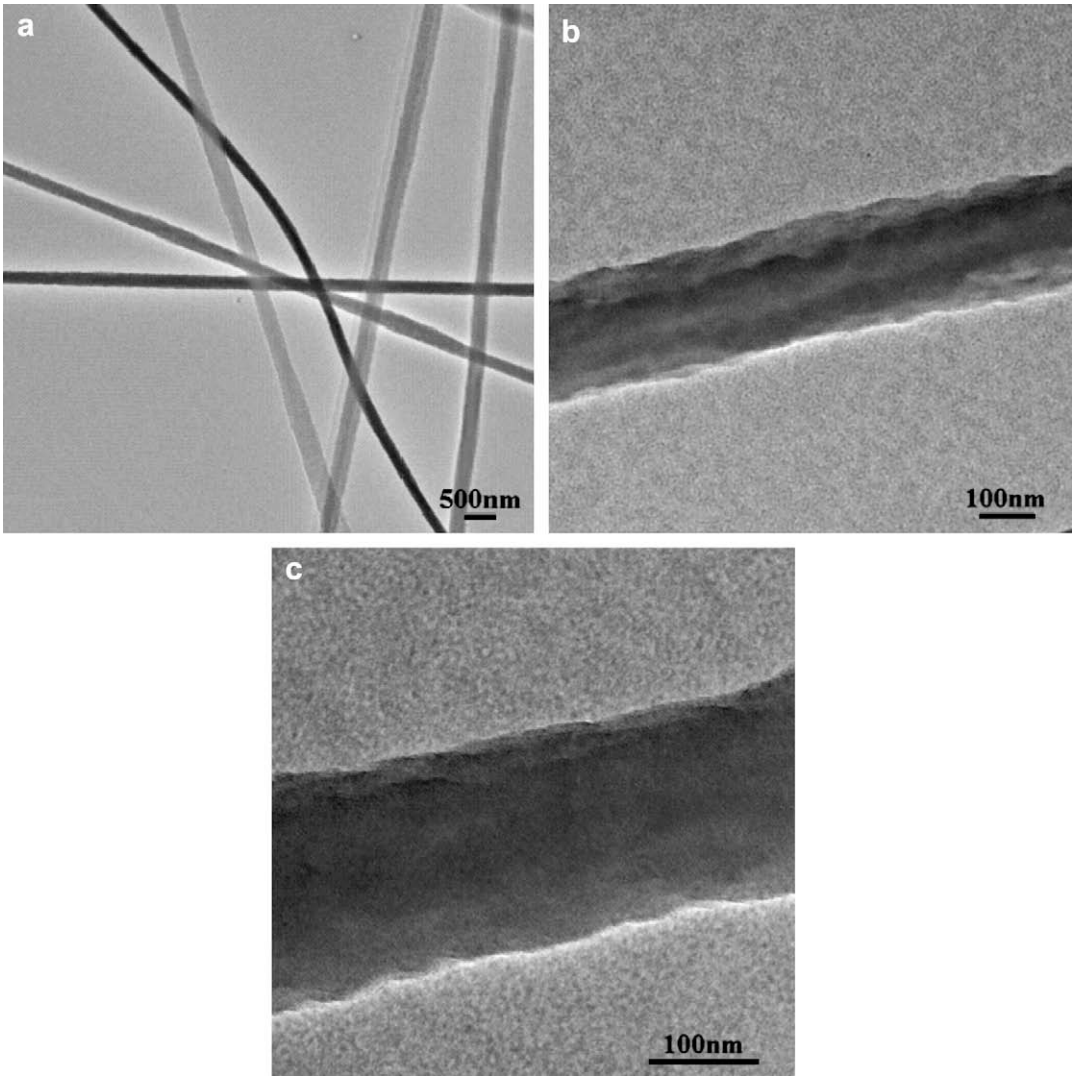

Fig. 2. TEM images of PAN/$ZnCl_2$ (10 wt%) composite nanofibers with different scale bars.

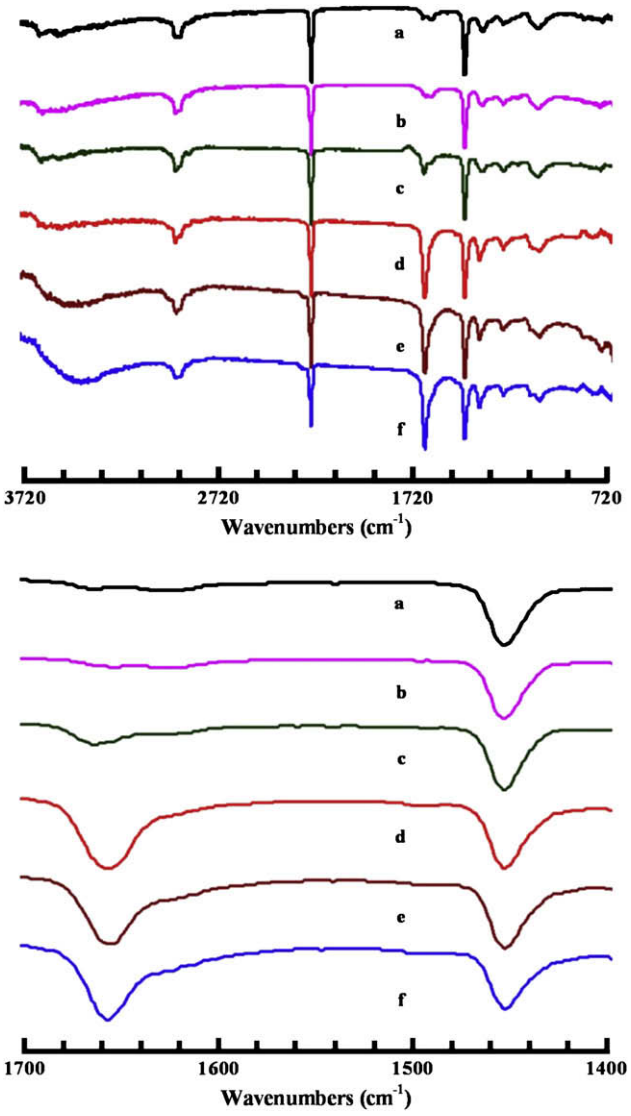

Fig. 3. ATR-FTIR spectra of PAN/$ZnCl_2$ composite nanofibers with different $ZnCl_2$ concentrations: (a) 0 (pure PAN), (b) 1, (c) 2, (d) 5, (e) 10, and (f) 15 wt%.

3.2. ATR-FTIR of PAN/$ZnCl_2$ composite nanofibers

ATR-FTIR spectra recorded in the spectral range of 3800–700 cm^{-1} are presented in Fig. 3. The spectrum of pure PAN nanofibers contains prominent peaks at around 2920, 2240, and 1450 cm^{-1} due to the stretching vibration of methylene and nitrile groups and the bending vibration of methylene, respectively [16,17]. The positions of these peaks in PAN/$ZnCl_2$ composite nanofibers shift to slightly lower values due to the interaction between PAN molecules and zinc ions. The peak intensity of the C=O stretching observed at about 1670 cm^{-1} increases greatly with increase in $ZnCl_2$ concentration. These phenomena indicate that $ZnCl_2$ salts and possibly the PAN molecules interact with the solvent DMF [18]. It is likely that these interactions are the cause of the changes in solution viscosity and surface tension discussed in the previous section.

3.3. Thermal analysis of PAN/$ZnCl_2$ composite nanofibers

Thermal studies of PAN/$ZnCl_2$ composite nanofibers were carried out using DSC and TGA. Fig. 4 shows the DSC thermograms

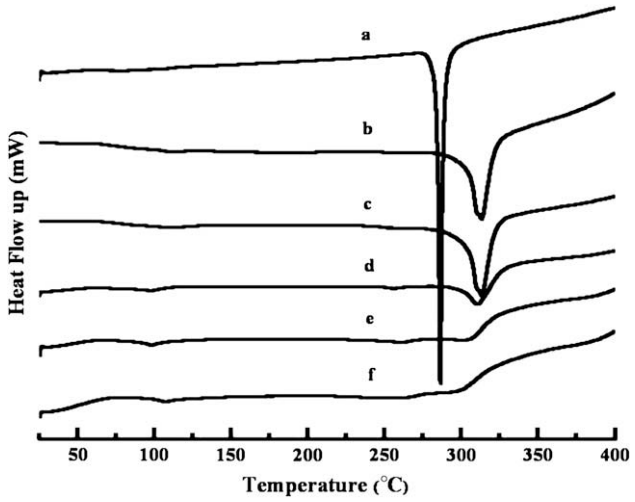

Fig. 4. DSC thermograms of PAN/$ZnCl_2$ composite nanofibers with different $ZnCl_2$ concentrations: (a) 0 (pure PAN), (b) 1, (c) 2, (d) 5, (e) 10, and (f) 15 wt%.

of PAN and PAN/$ZnCl_2$ nanofibers. Pure PAN nanofibers exhibit a relatively large and very sharp exothermic peak at about 290 °C and also an unobvious glass transition at about 106 °C [16]. At low $ZnCl_2$ concentrations (1, 2, and 5 wt%), the exothermic peak shifts to higher temperatures, and the peak becomes broader compared to pure PAN nanofibers. Additionally, the peak area intensity, which indicates the total heat of reaction, decreases as $ZnCl_2$ concentration increases. At higher $ZnCl_2$ concentrations (10 and 15 wt%), the exothermic peak becomes indistinguishable, while the glass transition becomes increasingly well defined.

It has been reported that the exothermic peak of PAN can result from three principal reactions, i.e., dehydrogenation, instantaneous cyclization, and crosslinking reactions, which are exothermic in nature [19]. Among these three reactions, the predominant one is the instantaneous cyclization reaction [16,19,20]. The large and sharp peak of pure PAN indicates the instantaneous cyclization of nitrile groups into an extended conjugated ring system in the nitrogen atmosphere [16,19]. The broadening of the exothermic

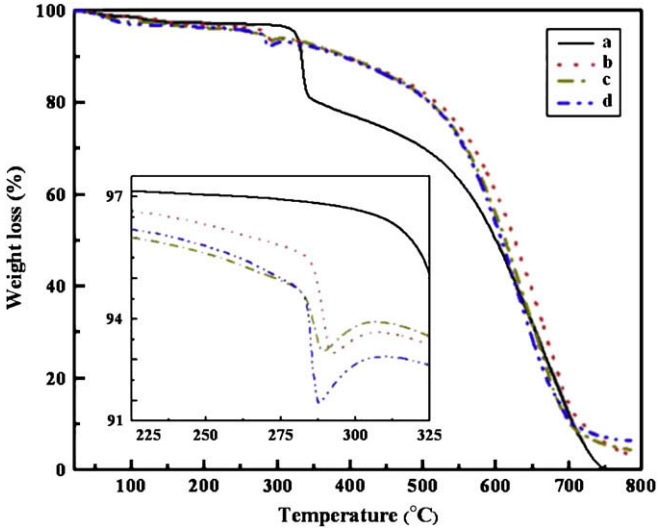

Fig. 5. TGA thermograms of PAN/$ZnCl_2$ composite nanofibers with different $ZnCl_2$ concentrations: (a) 0 (pure PAN), (b) 5, (c) 10, and (d) 15 wt%. Inset: detailed view of the decomposition between 225–325 °C.

peak in the presence of $ZnCl_2$ suggests that $ZnCl_2$ either works as a dehydration reagent, or modifies the activity of the free radicals involved in the cyclization reaction. The reduced reaction heat is caused by the interactions between PAN and $ZnCl_2$, which decrease the formation of free radicals on the nitrile groups and subsequently their recombinations. The shifting of the peak to higher temperatures is also attributed to the inhibiting effect of $ZnCl_2$ on the free radical formation. At higher $ZnCl_2$ concentrations, the exothermic peak disappears, indicating that the cyclization reaction may cease to occur because of the interactions between PAN molecules and large quantities of $ZnCl_2$ inhibitor. As a result, it can be concluded that the cyclization of PAN molecules in nitrogen environment is hindered by the addition of $ZnCl_2$ [20,21].

Thermo-gravimetric analysis (TGA) was also performed on the electrospun composite nanofibers in an air environment. As shown in Fig. 5, the weight loss of the composite nanofibers begins at a lower temperature compared with that of pure PAN nanofibers, and the percentage of weight lost in composite nanofibers is also much lower than that of pure PAN nanofibers. This may be the result of $ZnCl_2$ acting as a dehydrating agent, eliminating water and accelerating the oxidative stabilization reactions which are known to occur when PAN is thermally treated in an air environment [19,20]. From Fig. 5, it is also seen that there is no significant difference in the TGA curves of PAN/$ZnCl_2$ nanofibers with different $ZnCl_2$ concentrations, and the reason is not clear. More work is needed to understand the mechanism.

It is also important to note that the DSC measurements were only performed in nitrogen environment due to the equipment limitation. Further DSC studies of PAN/$ZnCl_2$ in air should be useful to definitively elucidate the nature of these thermal behaviors in PAN/$ZnCl_2$ nanofibers.

3.4. Exposure of PAN/$ZnCl_2$ nanofibers to H_2S

Polymer films made from nanoscale fibers exhibit high surface areas, which facilitate the diffusion of molecules and dopants into the fibrous material, and as a result, they are quite promising candidates to be used for chemical sensors of harmful reagents, such as H_2S [22,23]. In this study, the response of PAN/$ZnCl_2$ nanofibers to chemical reagents was directly investigated by exposing these fibers to an aqueous solution of H_2S.

Fig. 6 shows TEM images of PAN/$ZnCl_2$ (10 wt%) composite nanofibers after exposure to a H_2S aqueous solution (0.4 g H_2S per 100 ml), and it is seen that ZnS crystals are formed around the surface of the fibers, which will be further supported by ATR-FTIR, WAXD, and UV–vis spectrum data discussed later. From Fig. 6a it is

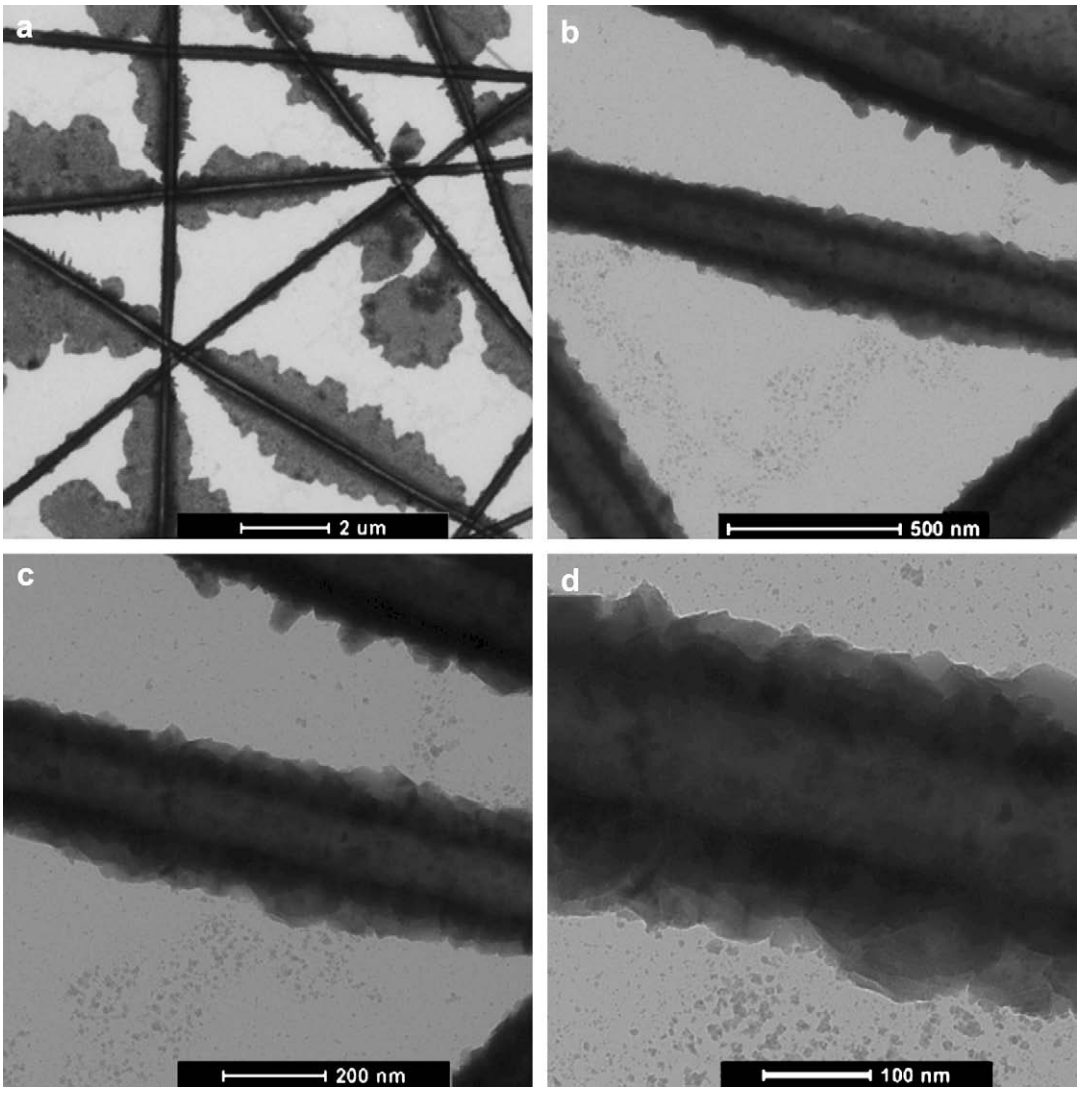

Fig. 6. TEM images of PAN/$ZnCl_2$ (10 wt%) composite nanofibers with different scale bars after exposing to H_2S aqueous solution.

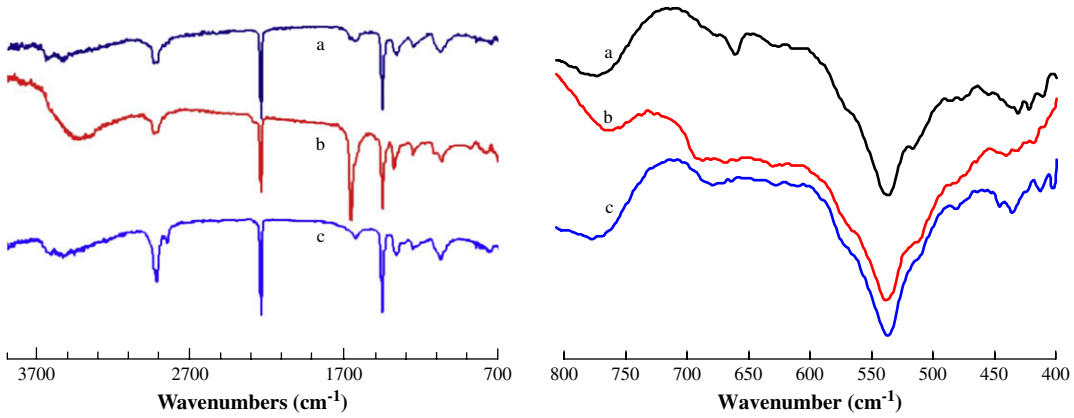

Fig. 7. ATR-FTIR spectra of pure PAN (a) and PAN/$ZnCl_2$ (10 wt%) composite nanofibers before (b) and after (c) exposing to H_2S aqueous solution.

seen that ZnS crystals can form in large quantities, growing quite far from the fiber surface. Fig. 6b–d also show the encapsulation of the fibers by the crystals although they are much smaller. A comparison of these images with those of untreated PAN/$ZnCl_2$ fibers (Fig. 2) reveals that the diameters of the fibers increase significantly after exposure to H_2S.

Nanofibers formed from PAN/$ZnCl_2$ solutions exhibit high accessible surface areas, which seem to be covered completely by ZnS crystals upon exposure to H_2S. Since ZnS is a direct wide band gap semiconductor with a large excitation binding energy and a small Bohr radius [12–14], this behavior suggests that PAN/$ZnCl_2$ nanofibers would likely gain semiconducting properties upon exposure to H_2S if the resultant ZnS can form a continuous semiconducting pathway along the fiber surface. Furthermore, the conversion of $ZnCl_2$ to semiconducting ZnS crystals indicates that these PAN/$ZnCl_2$ nanofibers might also be a good candidate to sense and/or remove H_2S from aqueous environments.

In order to prove the validity of ZnS formation upon the exposure of nanofibers to H_2S aqueous solution, ATR-FTIR and WAXD were employed to determine qualitatively the presence of ZnS semiconductor after H_2S treatment. The ATR-FTIR spectrum from 4000–400 cm^{-1} (Fig. 7) of PAN/$ZnCl_2$ (10 wt%) composite nanofibers shows a small stretching vibrational peak at around 2920 cm^{-1}, a strong C=O stretching frequency observed at about 1670 cm^{-1} and the characteristic band of O–H groups at 3400 cm^{-1} due to the interaction between PAN molecules and $ZnCl_2$ salt and the water absorbed into the $ZnCl_2$ salt. However, the H_2S-treated nanofibers show a strong, but slightly blue shifted peak at 2920 cm^{-1}, and an additional small peak at about 2850 cm^{-1} (just below 2920 cm^{-1}). A decrease in the intensities of the C=O and O–H peaks is also observed. This could be a result of the weakened coordinate link between –OH and Zn^{2+} as ZnS begins to aggregate in PAN nanofibers. In addition, a peak appears around 440 cm^{-1}, the characteristic frequency of ZnS [24,25].

Fig. 8 compares the WAXD spectra of pure PAN nanofibers with that of PAN/$ZnCl_2$ composite nanofibers after exposing to the H_2S solution. The peak at $2\theta = 17^\circ$ is the characteristic of the (200) crystal planes of PAN, while the H_2S-treated nanofibers shows two additional clear peaks at $2\theta = 29^\circ$ and 48°, which can be indexed to the well-known cubic crystal structure of ZnS [26,27].

UV–vis spectra of the PAN/ZnS nanofibers (Fig. 9) show an absorption edge at about 340 nm, which is attributed to ZnS crystals. With increase in ZnS concentration, the absorption edge shows a red shift, which is possibly the result of the increased size of ZnS crystals [28,29].

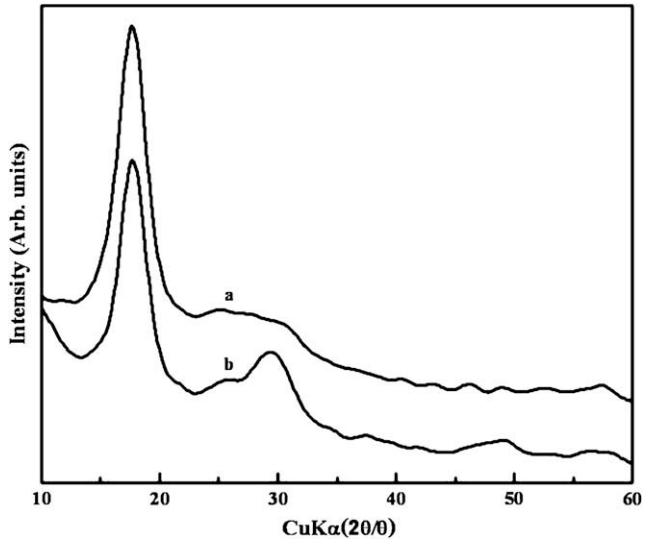

Fig. 8. WAXD spectra of pure PAN (a) and PAN/$ZnCl_2$ (10 wt%) composite nanofibers after exposing to H_2S aqueous solution (b).

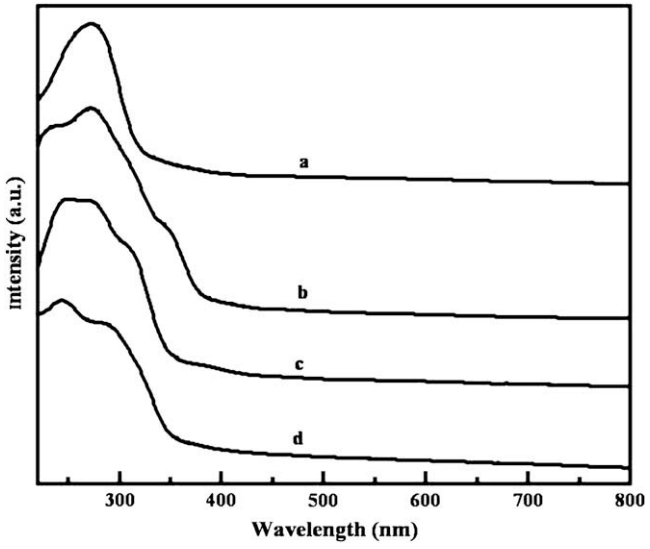

Fig. 9. UV–vis absorption spectra of PAN/ZnS composite nanofibers made from PAN/$ZnCl_2$ with different $ZnCl_2$ concentrations: (a) 0 (pure PAN), (b) 1, (c) 2, and (d) 10 wt%.

4. Conclusions

PAN/$ZnCl_2$ composite nanofibers containing different salt contents were successfully prepared through electrospinning. From SEM and TEM images, it is found that increasing $ZnCl_2$ concentration in the spinning solution reduces the fiber diameter, most likely due to the increased solution conductivity. ATR-FTIR spectra validate the presence of $ZnCl_2$ in nanofibers, and along with DSC and TGA curves, reveal that there are interactions among PAN chain, $ZnCl_2$ salt, and DMF solvent. These interactions have profound effects on the thermal properties of nanofibers.

Furthermore, it is found that, upon exposure to the aqueous H_2S solution, $ZnCl_2$ salts in PAN/$ZnCl_2$ composite nanofibers react with H_2S to form ZnS crystals on the fiber surface. This was confirmed using TEM, ATR-FTIR, XRD, and UV–vis spectra. These results suggest that PAN/$ZnCl_2$ nanofibers are potential candidates in H_2S sensing and removal, and further research should focus on determining the conversion efficiency of H_2S by the composite nanofibers, and also the sensitivity and the reaction rate in order to further explore potential applications.

Acknowledgements

This work was supported by the U.S. National Science Foundation (No. 0555959). The authors thank Professor Saad A Khan and Mr. Christopher A. Bonino in the Department of Chemical and Biomolecular Engineering at NC State University for their discussions during the experiments. The authors are also indebted to Dr. Dale Batchelor in the Analytical Instrumentation Facility at NC State University and Ms. Michelle Gignac and Dr. Mark D. Walters in the Shared Materials Instrumentation Facility at Duke University for their help in sample characterizations.

References

[1] Li D, Xia YN. Adv Mater 2004;16:1151.
[2] Greiner A, Wendorff JH. Angew Chem Int Ed 2007;46:5670.
[3] Reneker DH, Chun I. Nanotechnology 1996;7:216.
[4] Deitzel JM, Kleinmeyer J, Harris D, Tan NCB. Polymer 2001;42:261.
[5] Onozuka K, Ding B, Tsuge Y, Naka T, Yamazaki M, Sugi S, et al. Nanotechnology 2006;17:1026.
[6] Demir MM, Gulgun MA, Menceloglu YZ, Erman B, Abramchuk SS, Makhaeva EE, et al. Macromolecules 2004;37:1787.
[7] Lu X, Zhao Y, Wang C. Adv Mater 2005;17:2485.
[8] Lu XF, Zhao YY, Wang C, Wei Y. Macromol Rapid Commun 2005;26:1325.
[9] Bai J, Li YX, Yang ST, Du JS, Wang SG, Zhang CQ, et al. Nanotechnology 2007;18:305601.
[10] Thavasi V, Singh G, Ramakrishna S. Energy Environ Sci 2008;1:205.
[11] Hu Z, Srinivasan MP, Ni Y. Adv Mater 2000;12:62.
[12] Xiong Q, Chen G, Acord JD, Liu X, Zengel JJ, Gutierrez H, et al. Nano Lett 2004;4:1663.
[13] Huang Y, Lieber CM. Pure Appl Chem 2004;76:2051.
[14] Kolmakov A, Moskovits M. Annu Rev Mater Res 2004;34:151.
[15] Zheng JF, He AH, Li JX, Xu J, Han CC. Polymer 2006;47:7095.
[16] Ji LW, Saquing C, Khan SA, Zhang XW. Nanotechnology 2008;19:085605.
[17] Yue Z, Benak KR, Wang J, Mangun CL, Economy J. J Mater Chem 2005;15:3142.
[18] Phadke MA, Kulkarni SS, Karode SK, Musale DA. J Polym Sci Part B Polym Phys 2005;43:2074.
[19] Kim J, Kim YC, Ahn W, Kim CY. Polym Eng Sci 1994;33:1452.
[20] Dalton S, Heatley F, Budd PM. Polymer 1999;40:5531.
[21] Giunta PR, Burgt LJ, Stiegman AE. Chem Mater 2005;17:1234.
[22] Virji S, Huang JX, Kaner RB, Weiller BH. Nano Lett 2004;4:491.
[23] Virji S, Fowler J, Baker C, Huang J, Kaner RB, Weiller B. Small 2005;1:624.
[24] Wang HY, Zhao YY, Li ZY, Lu XF, Wang C, Wei Y. Solid State Phenom 2007;121–123:641.
[25] Zhao L, Gao L. J Mater Chem 2004;14:1001.
[26] Zhang J, Han B, Liu D, Chen J, Liu Z, Mu T, et al. Phys Chem Chem Phys 2004;9:2391.
[27] Liu H, Kameoka J, Czaplewski DA, Craighead HG. Nano Lett 2004;4:671.
[28] Zhou Z, He DW, Xu WB, Ren FM, Qian YT. Mater Lett 2007;61:4500.
[29] Zhao Y, Wang F, Fu Q, Shi W. Polymer 2007;48:2853.